

Design and simulation of novel flow field plate geometry for proton exchange membrane fuel cells

Hanxia Ruan¹ · Chaoqun Wu² · Shuliang Liu² · Tao Chen²

Received: 10 February 2015 / Accepted: 5 December 2015 / Published online: 11 December 2015
© Springer-Verlag Berlin Heidelberg 2015

Abstract Bipolar plate is one of the many important components of proton exchange membrane fuel cell (PEMFC) stacks as it supplies fuel and oxidant to the membrane-electrode assembly (MEA), removes water, collects produced current and provides mechanical support for the single cells in the stack. The flow field design of a bipolar plate greatly affects the performance of a PEMFC. It must uniformly distribute the reactant gases over the MEA and prevent product water flooding. This paper aims at improving the fuel cell performance by optimizing flow field designs and flow channel configurations. To achieve this, a novel biomimetic flow channel for flow field designs is proposed based on Murray's Law. Computational fluid dynamics based simulations were performed to compare three different designs (parallel, serpentine and biomimetic channel, respectively) in terms of current density distribution, power density distribution, pressure distribution, temperature distribution, and hydrogen mass fraction distribution. It was found that flow field designs with biomimetic flow channel perform better than that with convectional flow channel under the same operating conditions.

1 Introduction

Proton exchange membrane fuel cell (PEMFC) is a power equipment which converts chemical energy in fuel

(generally is hydrogen) and oxidant (generally is oxygen in air) into electrical energy. It is considered to be very promising new energy equipment in the twenty first century since its favorable characteristics such as high efficiency, environmentally friendly, wide adaptation to working environment, fuel flexibility and higher power density. Many countries, enterprises and scientific research institutions are devoting themselves in the research and development. Today, the technology of PEMFC is more and more mature, and its utility also becomes more and more popular in our daily life [1–4].

As new energy equipment, compared with the traditional power equipments, PEMFC has obvious superiority. However, at present its development and utility are less popular than the traditional power equipments such as internal combustion engine, metal battery. The reasons are various, but with the deepening of the research and advances in technology related, it will become increasingly widespread. Current research of PEMFC has been centering on improving the output performance, increasing safety, improving longevity and stability [5, 6]. The performance of the PEMFC can be improved by optimizing its operating parameters, such as gas flow rate, operating cell temperature, inlet pressure, humidity condition, and flow channel type. This paper aims to study and improve the structure of PEMFC bipolar plates to achieve the purpose of enhance the performance of PEMFC.

The flow channel on the bipolar plate in PEMFC is the gas transmission channel and water removal channel, whose shape and size plays a critical role of its performance. The design of the flow channel on bipolar plates mainly focuses on three aspects: the flow channel distribution pattern [7–13], the cross-section shape [14–16] and the land and channel dimensions [17–20]. Researcher still continuously innovate and develop new flow field

✉ Chaoqun Wu
chaoqunwu@whut.edu.cn

¹ School of Material Science and Engineering, Wuhan University of Technology, Wuhan 430070, China

² School of Mechanical and Electronic Engineering, Wuhan University of Technology, Wuhan 430070, China

structure. Biomimetic flow field is a new flow field structure based on the biological structure in nature [21]. Through observing the features of the biological structures, a series of rules have been summarized and applied to the design of flow field structure so as to improve the PEMFC performance. The newly designed biomimetic flow field by Currie [22], compared to conventional flow field, has higher average current density and more uniform distribution of current density as well. Kjelstru et al. [23] finds that the current density of H type flow field, under the same condition ($20\% \text{PtC}^{-1}$), increases by 10–20 % over conventional flow fields. Kloess et al. [24] design two different flow fields: the lung flow field and the biomimetic flow field. Within their research, both numerical simulation and experimental method are employed to compare the performances of the new structures with that of the conventional flow field structures. From the results, it is found that both the lung flow field and biomimetic flow field have lower pressure drop between inlet and outlet and more even velocity distribution in diffusion layer, which is beneficial to reacting evenly. Wang et al. [25] design a new biomimetic flow channel to improve the PEMFC performance. Two dimensional numerical simulation was committed to the new biomimetic flow channel and traditional flow channel at $Re = 10, 100$ respectively. Besides, 3-D numerical simulation concerns the channel ratio was done. The results show that the biomimetic flow field has more even velocity distribution and lower pressure loss. Biomimetic flow channels perform better when evaluated either by the Renault value or from the channel ratio aspect. After testing the performance of the parallel flow field, the serpentine flow field and two new bio-inspired flow fields, Wang et al. [26] find that the new biomimetic flow fields possess higher gas consumption efficiency and higher water removal efficiency. In order to test the performance of different flow fields, a 25 cm^2 fuel cell was assembled and tested for four different flow channels: serpentine, interdigitated, lung and biomimetic flow channel. The results show that lung flow field and the biomimetic flow field possess better fuel cell performance, and that the current densities of them increase nearly by 30 % over the conventional flow fields.

In the present work, a novel biomimetic flow field designs by mimicking the structures of leaf veins has been proposed to achieve higher PEMFC performance. Computational fluid dynamics (CFD) based simulations were conducted to compare three different configurations (parallel, serpentine and biomimetic channel, respectively) at different operation variables. It was found that flow field designs with biomimetic flow channel perform better than that with convectional flow channel under the same operating conditions.

2 Nature inspired flow field designs

The flow field design of a bipolar plate greatly affects the performance of a PEMFC. It must uniformly distribute the reactant gases over the MEA and prevent product water flooding. The flow field design involves the layout of the flow field and channel cross-section geometries including shape and dimensions. The leaves found in nature are considered a natural optimization of the enhanced heat transfer and mass transfer of flow channel. They have a uniform distribution of microtubules and facilitate the energy and material delivery. The mass transfer and heat transfer of PEMFC bipolar plate is similar to leaves. The flow field distribution in PEMFC bipolar plate can be regarded as a self-growth process like leaf vein formation, thus flow field is started from a given “seed” and is grown, branched off or degenerated according to a certain growing rule, to form the optimal distribution patterns. In this paper, the flow field design is inspired by the distribution of leaf veins, and the channel dimensions are calculated using Murray’s Law.

2.1 The structure of a leaf

Living things in nature are evolutionary, and survivors can adapt to environment well. Plant is one of the survivors, most of which rely on leaves to grow. Both leaves and their veins are in different shapes, as we can see in Fig. 1.

Veins, the vascular bundles in leaves, are the branches of vascular stems. The vascular bundles always distribute along the petiole in some form of special shape. The large and obvious vein, locating in the center of leaf, is called the midrib or main vein (Mid vein). And the smaller veins distributed along main vein are called the lateral veins (Lateral veins). The small veins or veinlets (Minor veins) (shown as in Fig. 1b) are the smallest bundles on the leaf which distribute all over the leaves. Those veins are the transport channel of water, salts and the output of photosynthetic products in plants [27]. As outstanding product of nature, these different patterns of veins undoubtedly have good biological and physico-chemical properties, and also they can be good at transferring material and supporting blades. These characteristics meet the requirements of the flow channel in PEMFC which demand good circulation and mechanical properties.

2.2 Murray’s law

In 1926, Murray [28] put forward the famous Murray’s Law after his fully study and analysis of physiological bifurcation systems. Murray’s Law reveals that if the diameters of the mother pipe and branches of a bifurcate system are in charge of special proportion, the consumption of energy and

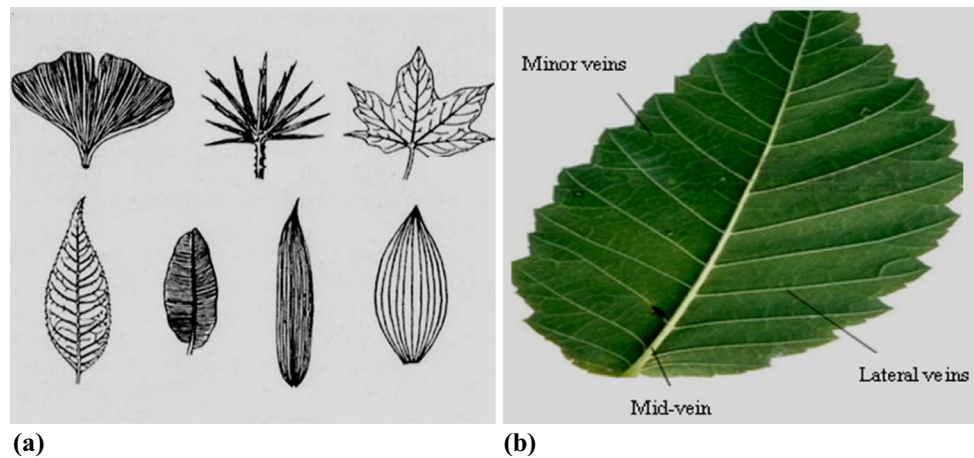


Fig. 1 The schematic and physical diagram of leaves. **a** The schematic diagram of leaf, **b** the pinnately physical diagram of leaf

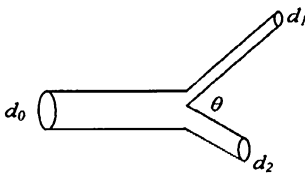


Fig. 2 The schematic diagram of single bifurcation structure

the pressure drop can be relative small when the fluid flows through the system. Murray's Law has been demonstrated in a series of natural bifurcate systems since it was advanced. Its development and derivation is still going on, and gradually used to guide the design of fluid flow channel.

$$d_0^3 = d_1^3 + d_2^3 \quad (1)$$

$$d_0^3 = \sum_{k=1}^m d_k^3 \quad (2)$$

For bifurcate structure (shown as Fig. 2), the relationship between the diameter of parent tube and diameters of branches can be described by Eq. (1), in which d_0 represents the diameter of parent tube, d_1 , d_2 represent the diameters of branches, respectively; And the further derivation of the relationship between the diameter of parent tube and diameters of branches of multi-branch systems can be described by Eq. (2), in which the subscript k indicates the k th pipe, and m means the number of pipes. While $d_1 = d_2$, the following Eq. (3) can be derived:

$$d_1 = d_2 = 2^{-1/3} d_0 \quad (3)$$

The processes are the theoretical derivation of Murray's Law, and Eqs. (1), (2) are all the manifestations of Murray's

Law. Since there are no restrictions of the symmetry of the system and numbers of branches of the bifurcate system for the derivation of Murray's Law, so Murray's Law is also applicable to asymmetric and multi-branch system [29].

2.3 Biomimetic flow channel

The prototype of the biomimetic flow channel in the article is the naturally pinnate vein (shown as in Fig. 1b), and the dimensions of the channel are calculated by Murray's Law. Based on pinnate vein, the main vein and lateral veins have been simplified into rectangular cross-section mainstream channel and secondary channels. The symmetric sub-channels are distributed along the center axis of the main channel, and arranged by the main channel at an angle in parallel. Research shows that the symmetric flow channel can promote the internal distribution of pressure more evenly to improve performance of PEMFC [30].

The dimensions of flow channel generally consist of width, height and width of the rib, which are critical for the performance of PEMFC as well. This article bases on reference of previous studies and combines with Murray's Law to get the dimensions. Generally in current researches the dimensions of the flow channel as: width is between 0.5 and 3 mm; rib width is between 0.5 and 3 mm; depth is between 0.2 and 2.5 mm. Also, considering that the cross-section of the channels is rectangular and the ratios of width to depth of the secondary channels are around 1, the design has taken the widths of the channels as equivalent diameter. The ratios of the width between the main channel and sub-channels are 2:1. In order to improve the design further to make the flow channels more similar to the distribution of the plant veins, the third-level channels have been added into the flow channel. And, the distances between the third-level channels and the symmetry axis are respectively

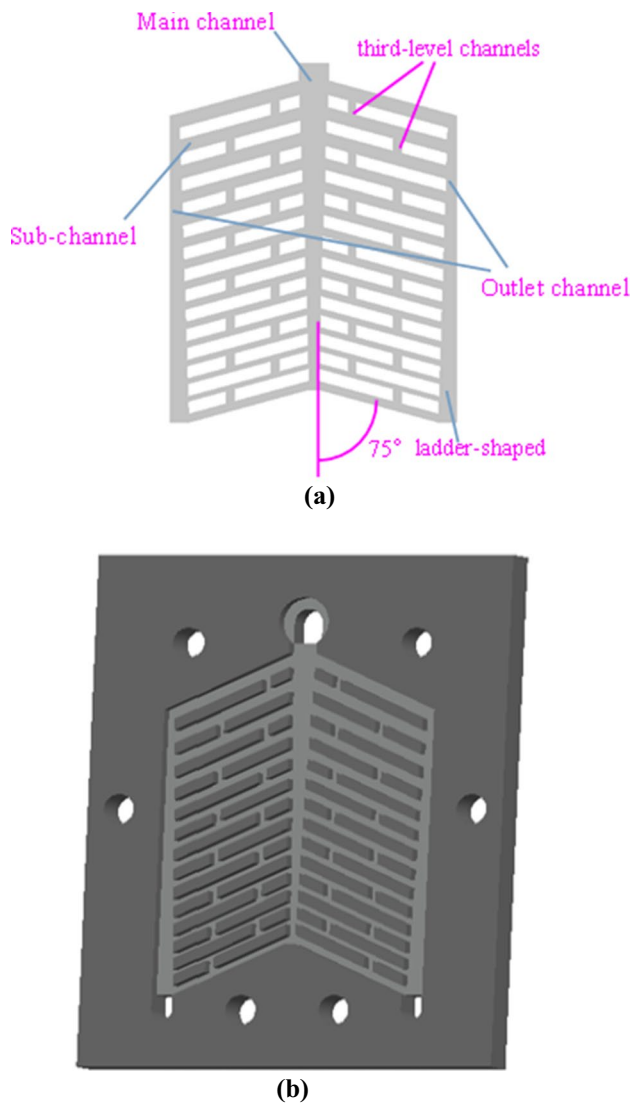


Fig. 3 Biomimetic flow channel. **a** 2-dimensional diagram, **b** physical diagram

3.5 and 7.5 mm. Meanwhile, in order to increase the outlet pressure to facilitate the discharge of product, the shape of the outlet channel has been changed from rectangular cross-section to ladder-shaped. The angle between the sub-channels and the symmetry axis in flow field is 75 degrees based on Murray's Law [31] (shown as Fig. 3).

2.4 Conventional flow channels

In order to investigate the advantages of a newly proposed biomimetic flow channel, the comparison with conventional flow channels is conducted in this paper. The conventional flow channels are parallel channel and serpentine channel which are commonly used in PEMFC. The dimensions of the channels are as follow, parallel channel: width

is 0.9 mm, rib of width is 1 mm, and depth is 1 mm (shown as in Fig. 4a); serpentine channel: width is 1 mm, width of rib is 1 mm, and depth is 1 mm (shown as in Fig. 4b).

3 Mathematic model

3.1 Model assumptions

The present model assumes:

- ideal gas mixtures;
- steady state conditions;
- the flow is laminar;
- system is isothermal;
- fluid is incompressible;
- fuel cell porous zones are isotropic.

3.2 Model equations

In the current three-dimensional mathematical model of PEMFC, the basic governing equations [32], which include mass conservation equation, mass transfer equation, momentum conservation equation, energy conservation equation, species conservation equation and current conservation equation, are the foundation of numerical simulation.

$$\nabla(\varepsilon\rho\vec{u}) = S_m \quad (4)$$

$$\nabla(\varepsilon\rho\vec{u}C_k) = -\nabla J_k + S_k \quad (5)$$

$$\nabla(\varepsilon\rho\vec{u}\vec{u}) = -\varepsilon\nabla p + \nabla(\phi\mu\nabla\vec{u}) + S_u \quad (6)$$

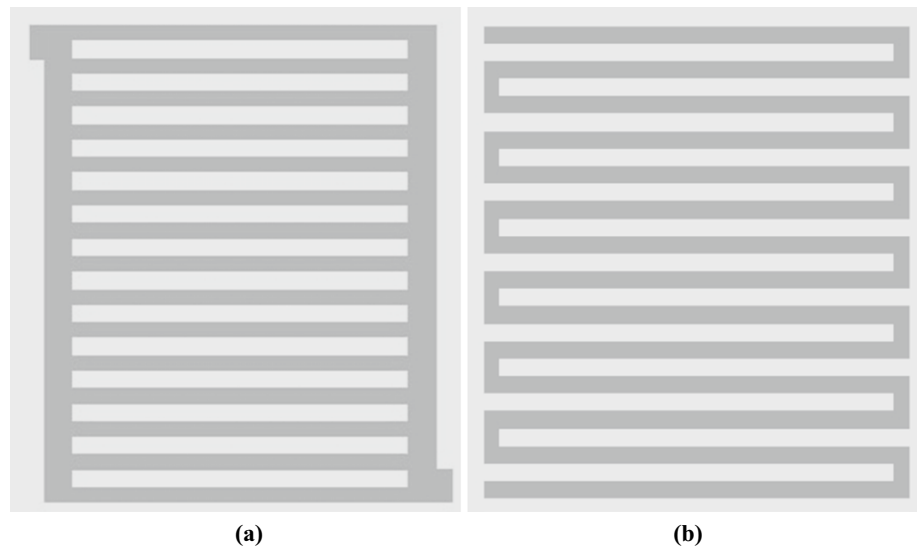
$$\frac{\partial(\varepsilon\rho c_p T)}{\partial t} + \nabla(\varepsilon\rho c_p\vec{u}T) = \nabla(k^{eff}\nabla T) + S_Q \quad (7)$$

$$\frac{\partial(\varepsilon c_k)}{\partial t} + \nabla(\varepsilon c_k\vec{u}) = \nabla(D_k^{eff}\nabla c_k) + S_k \quad (8)$$

$$\nabla(\sigma_e\nabla\phi_e) + S_e = 0 \nabla(\sigma_m\nabla\phi_m) + S_m = 0 \quad (9)$$

here ε is porosity, ρ is density, \vec{u} is velocity vector, S_m is source item of the mass, C_k is species concentration of species k , J_k is the diffusion flux of species k , S_k is source item of mass changes, μ is the viscosity; S_u is the momentum source item; C_p as specific heat at constant pressure, T is the temperature; S_Q is energy source item, S_k is source item of species, p is pressure; k^{eff} is the effective thermal conductivity coefficient, D_k^{eff} is effective diffusion coefficient of species, σ is the conductivity. The water transfer in proton

Fig. 4 Conventional flow channels. **a** Parallel-channel, **b** serpentine-channel



exchange membrane (PEM) is affected by electro-osmosis (J_d), diffusion transfer (J_p) and infiltration transfer (J_p). Therefore the net water content inside the PEM is decided by the algebraic sum of the above-mentioned phenomenon. Water flux of membrane (J_w) is as follow:

$$J_w = J_d + J_c + J_p = n_d \frac{I}{F} - D_m \frac{\partial c}{\partial y} + D_p \frac{dp}{dy} \quad (10)$$

Within the equation, I is current density, F is the Faraday constant, c is concentration, D_m diffusion coefficient, D_p as the pressure migration coefficient, n_d is electric migration coefficient, the expression is as follow:

$$n_d = \frac{2.2}{25} \lambda \quad (11)$$

The relationship between λ and water saturation α is as follow:

$$\lambda = 0.043 \quad (\alpha < 0)$$

$$\lambda = 0.043 + 17.81\alpha - 39.85\alpha^2 + 36\alpha^3 \quad (0 \leq \alpha < 1)$$

$$\lambda = 14.0 + 1.4(\alpha - 1) \quad (1 \leq \alpha \leq 3)$$

$$\lambda = 16.8 \quad (\alpha > 3)$$

α is the water saturation and described as:

$$\alpha = \frac{P_w}{P_{sat}(T)} + 2s \quad (12)$$

P_w is the local water vapor pressure, $P_{sat}(T)$ is the saturation pressure which can be obtained through local saturation vapor pressure instrument, s is the saturation of liquid water.

$$D_m = D_\lambda \exp \left[2416 \left(\frac{1}{303} - \frac{1}{T} \right) \right] \quad (13)$$

where,

$$D_\lambda = 10^{-10} \quad (\lambda < 2)$$

$$D_\lambda = 10^{-10} \times [1 + 2(\lambda - 2)] \quad (2 \leq \lambda \leq 3)$$

$$D_\lambda = 10^{-10} \times [3 - 1.67(\lambda - 3)] \quad (3 < \lambda < 4.5)$$

$$D_\lambda = 1.25 \times 10^{-10} \quad (\lambda \geq 4.5)$$

3.3 Boundary conditions and modeling parameters

The computational domain of simulation includes bipolar plates, flow channel, anode and cathode diffusion layer, anode and cathode catalyst layer and proton exchange membrane. Electrode and membrane parameters are shown in Table 1, geometrical and operating parameters are shown in Table 2. The boundary conditions of the inlet and outlet of flow channel for calculation are specified with mass flow inlet and pressure outlet respectively. Anode and cathode mass flow rate m_{an} and m_{cat} can be calculated by the following equations:

$$m_{an} = \left(\frac{M_{H_2} \times I_{ref} \times A}{2F} \right) \times \zeta_a / m_{H_2} \quad (14)$$

$$m_{cat} = \left(\frac{M_{O_2} \times I_{ref} \times A}{2F} \right) \times \zeta_c / m_{O_2} \quad (15)$$

3.4 Numerical solution of equations

The governing equations along with their appropriate boundary conditions, are discretized by the finite volume method and solved in the commercial CFD software package, Fluent (version 6.3). The source terms and physical properties are

Table 1 Electrode and membrane parameters

Parameter	Value
Anode reference current density (A/m^2)	10,000
Cathode reference current density (A/m^2)	20
Anode reference concentration ($kmol/m^3$)	1
Cathode reference concentration ($kmol/m^3$)	1
Anode concentration exponential	0.5
Cathode concentration exponential	1
Anode volumetric reference exchange current density (A/m^3)	1.5×10^9
Anode volumetric reference exchange current density (A/m^3)	4×10^6
Anode exchange coefficient	2
Cathode exchange coefficient	2
Anode reference concentration ($kmol/m^3$)	1
cathode reference concentration ($kmol/m^3$)	1
Hydrogen reference diffusivity (m^2/s)	3×10^{-5}
Vapor reference diffusivity (m^2/s)	3×10^{-5}
Oxygen reference diffusivity (m^2/s)	3×10^{-5}
Other species reference diffusivity (m^2/s)	3×10^{-5}
Catalyst layer surface-to-volume ration ($1/m^2$)	2×10^5
Catalyst layer effective conductivity ($1/ohm\ m$)	5000
Diffusion layer porosity	0.5
Catalyst layer porosity	0.5
Diffusion layer viscous resistance ($1/m^2$)	1×10^{12}
Catalyst layer viscous resistance ($1/m^2$)	1×10^{12}
Catalyst layer viscous resistance ($1/m$)	2×10^5
Membrane equivalent weight ($kg/kmol$)	1100
Membrane protonic conduction coefficient	1
Membrane protonic conduction exponent	1
Membrane thermal conductivity ($W/m\ K$)	2
Membrane specific heat at constant pressure ($j/kg\ K$)	2000
Membrane porosity	0.5
Membrane density (kg/m^3)	1790
Bipolar effective conductivity ($1/ohm\ m$)	1×10^6
Bipolar specific heat at constant pressure ($j/kg\ K$)	871
Bipolar thermal conductivity ($W/m\ k$)	8
Bipolar density (kg/m^3)	2719

implemented in a UDF user-defined function and the species and charge transport equations are solved through the software's user-defined scalars. The software utilizes the well-known SIMPLE (semi-implicit pressure linked equation) algorithm, and an algebraic multigrid solver to efficiently solve the resulting set of discretized linear equations [33]. The model solving process tends to converge when the relative error between two iterations is $<10^{-6}$.

Table 2 Geometrical and operational parameters

Parameter	Value
Channel height (mm)	1
Rib width (mm)	1
Diffusion layer thickness (mm)	0.2
Catalyst layer thickness (mm)	0.02
Membrane thickness (mm)	0.04
Active area (cm^2)	7.2
Anode inlet relative humidity (RH)	30 %
Cathode inlet relative humidity (RH)	60 %
Stoichiometry for anode	1.5
Stoichiometry for cathode	2
Anode inlet mass velocity (kg/s)	6.092×10^{-6}
Cathode inlet mass velocity (kg/s)	4.892×10^{-7}
Anode inlet temperature (K)	353
Cathode inlet temperature (K)	353
Operation temperature (K)	353
Operation pressure (atm)	1
Open-circuit voltage (V)	1.17

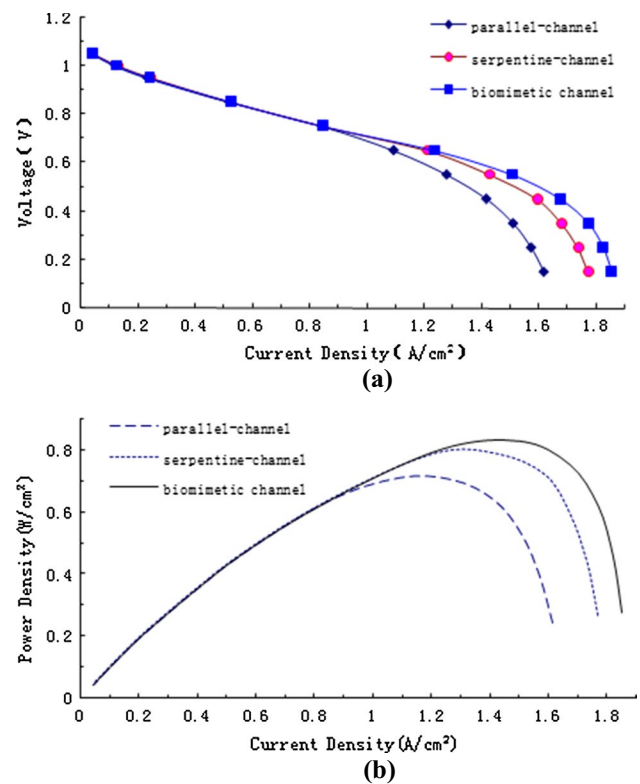


Fig. 5 Comparisons of polarization curves and power density curves for different flow field designs. **a** Polarization curves, **b** power density curves

4 Result and discussion

There are various factors that affect the performance of PEMFC, and this paper aims at improving its flow field structure to enhance the performance. In general, the performance of PEMFC can be judged by the characteristics of I - V curve, power density, mass transfer, dynamics and longevity.

In this paper, the simulation data are reprocessed by post-process software, i.e. Tecplot. To analyze the performance of PEMFC, this paper set output performance (including I - V curve, power density) and the distribution of reactants and products (including pressure/heat/water/hydrogen/current density distribution, as well as water content in membrane) to be the criterions for judging.

4.1 Output performance

The output performance is one of the most critical characteristics for PEMFCs. In theory, the output performance can be indicated by the current and voltage (I - V) polarization curves and the power density curves. Figure 5 has shown the I - V polarization curves and the power density curves of the three flow fields with different channels. In the figure, it can be seen that the output performance of the biomimetic flow channel is better than the conventional flow channel, especially in low operating voltage. For the biomimetic flow channel, it can be seen that when the operating voltage is 0.65 v, the PEMFC has the maximum output power. The following contrastive analysis is based on the simulation data in anode of PEMFC when operating voltage is 0.65,

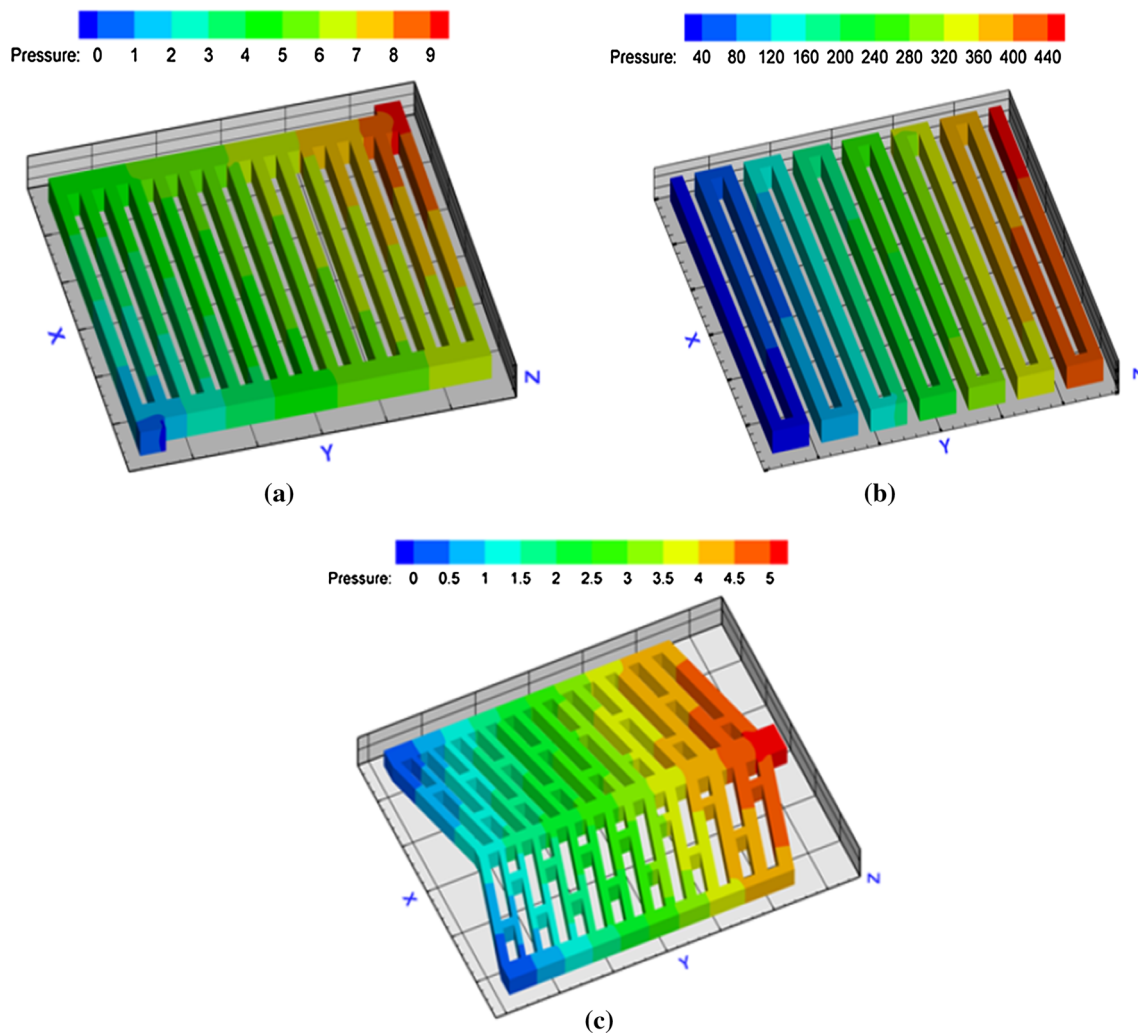


Fig. 6 Pressure distributions for different flow field designs. **a** Pressure distributions for parallel-channel, **b** pressure distributions for serpentine-channel, **c** pressure distributions for biomimetic flow channel

thus to analyze the role of the biomimetic flow channel in improving the performance of PEMFC.

4.2 Distribution of reactants and products

By comparing (a), (b), (c), in Fig. 6, the pressure drop observed in the serpentine flow channel is larger than other flow channels under the operating voltage. While the biomimetic flow channel has the smallest pressure drop and the most uniform distribution of pressure, which can be conducive to the stability of the output of power and the discharge of products.

As it's shown in Fig. 7: the distribution of temperature in (a) is the most uneven, the high temperature regions are also the widest; (b) and (c) show that the distribution of temperature is relatively lower and uniform and the regions with high temperatures are in the vicinity of the outlet. So the biomimetic flow channel is better than the conventional flow channel for PEMFC.

Liquid water can build up and stagnate in the flow channels. This reduces the flow of oxidizer to the cathode and reduces the overall efficiency of the fuel cell. Water, a product of the fuel cell reaction, must also be removed from the cathode side to prevent congestion, or flooding, in the oxidizer flow channels. Water mass fractions in the channels for different flow field designs were shown in Fig. 8. The biomimetic flow channel appears to have the best water management capabilities. For the biomimetic flow channel Fig. 8 indicates that most of the liquid water is formed in the outlet channels which mean it will be easy to remove from the system.

Figure 9 presents hydrogen mass fraction distribution for different flow field designs. As it can be seen in this figure, the biomimetic flow channel has the higher hydrogen mass fraction and more uniform hydrogen distribution. The higher the hydrogen mass fraction the better because it leads to increased reaction rate, and the uniform hydrogen distribution leads to even current density across the fuel cell.

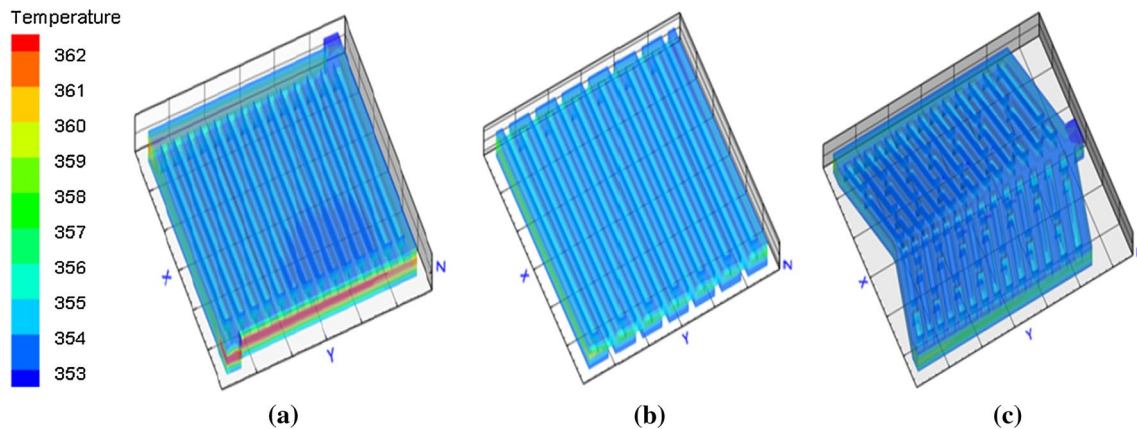


Fig. 7 Temperature distributions for different flow field designs. **a** Temperature distributions for parallel-channel, **b** temperature distributions for serpentine-channel, **c** temperature distributions for biomimetic flow channel

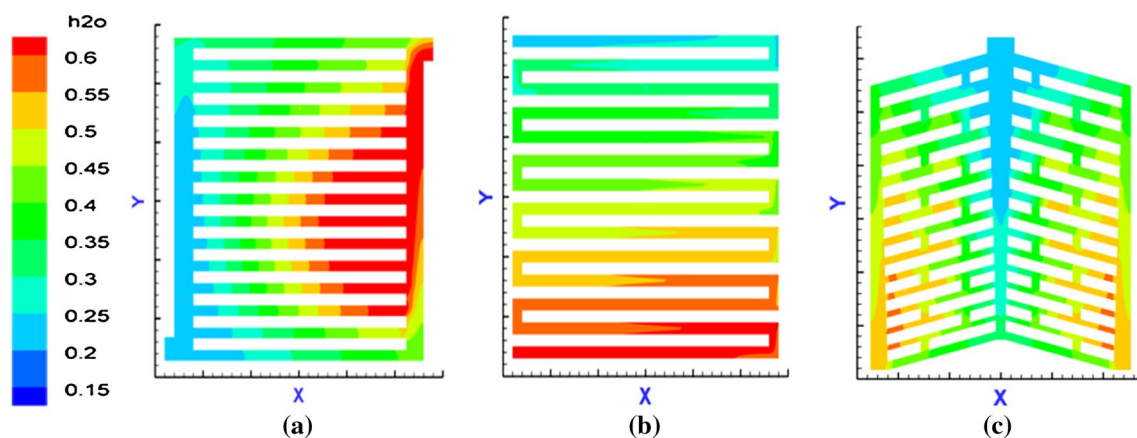


Fig. 8 Water mass fractions in the channels for different flow field designs. **a** Water mass fractions for parallel-channel, **b** water mass fractions for serpentine-channel, **c** water mass fractions for biomimetic flow channel

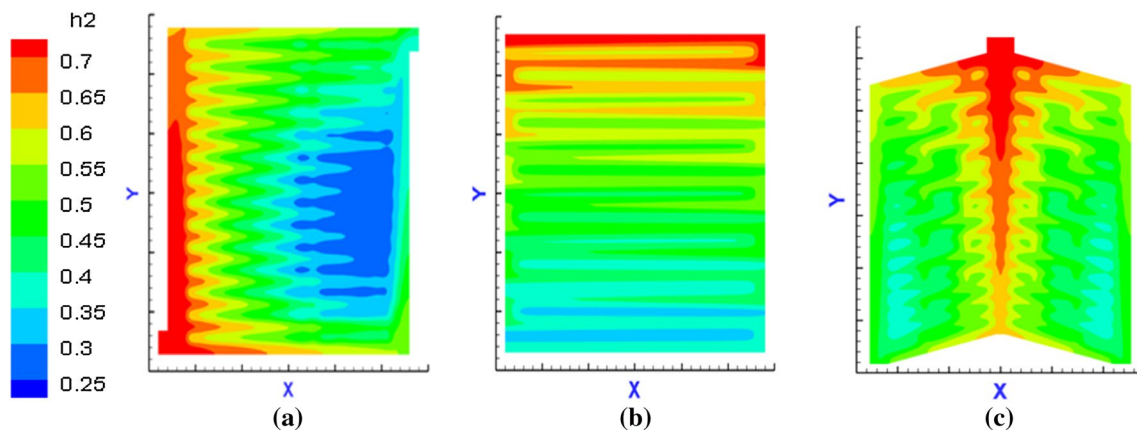


Fig. 9 Hydrogen mass fraction distribution for different flow field designs. **a** Hydrogen mass fractions for parallel-channel, **b** hydrogen mass fractions for serpentine-channel, **c** hydrogen mass fractions for biomimetic flow channel

5 Conclusion

The structure of the flow fields in PEMFC has a significant impact on its performance. This paper, a novel biomimetic flow channel has been proposed for the design of flow fields in order to achieve higher PEMFC performance. By comparing three different configurations (parallel, serpentine and biomimetic channel, respectively) in terms of current density distribution, power density distribution, pressure distribution, temperature distribution, and hydrogen mass fraction distribution leads to the conclusion that the proposed biomimetic flow channel can improve the output of power, and internally, the distribution of reaction gases is more uniform in the channel and the excess product of the chemical reaction is easier to remove from PEMFC.

Acknowledgments The authors would like to thank the National Science Foundation of China (Grant Numbers: 51575413 and 51305315) for funding this study.

References

1. Aiyejina A, Sastry MKS (2012) PEMFC flow channel geometry optimization: a review. *J Fuel Cell Sci Technol* 9:011011-1–01101124
2. Wee JH (2007) Applications of proton exchange membrane fuel cell systems. *Renew Sustain Energy Rev* 11:1720–1738
3. Wang Y, Chen K, Mishler J et al (2011) A review of polymer electrolyte membrane fuel cells technology, applications, and needs on fundamental research. *Appl Energy* 88:981–1007
4. Horde T, Achard P, Metkemeijer R (2012) PEMFC application for aviation: experimental and numerical study of sensitivity to altitude. *Int J Hydrog Energy* 37:10818–10829
5. Bruijn FA, Dam VAT, Janssen GJM (2008) Durability and degradation issues of PEM fuel cell components. *Fuel Cells* 8(1):3–22
6. Zhang L, Chae S, Hendren Z et al (2012) Recent advances in proton exchange membranes for fuel cell applications. *Chem Eng J* 204–206:87–97
7. Ratlamwala TA, El-Sinawi AH, Gadalla MA et al (2012) Performance analysis of a new designed PEM fuel cell. *Int J Energy Res* 36:1121–1132
8. Yan WM, Liu HC, Soong CY et al (2006) Numerical study on cell performance and local transport phenomena of PEM fuel cells with novel flow field designs. *J Power Sources* 161:907–919
9. Xu C, Zhao TS (2007) A new flow field design for polymer electrolyte-based fuel cells. *Electrochem Commun* 9:497–503
10. Su A, Chiu YC, Weng FB (2005) The impact of flow field pattern on concentration and performance in PEMFC. *Int J Energy Res* 29:409–425
11. Kim S, Shimpalee S, Zee Van (2005) Effect of flow field design and voltage change range on the dynamic behavior of PEMFCs. *J Electrochem Soc* 152:A1265–A1271
12. Ferng YM, Ay Su, Lu SM (2008) Experiment and simulation investigations for effects of flow channel patterns on the PEMFC performance. *Int J Energy Res* 32:12–23
13. Yang WJ, Kang SJ, Kim YB (2012) Numerical investigation on the performance of proton exchange membrane fuel cells with channel position variation. *Int J Energy Res* 36:1051–1064
14. Kumar A, Reddy RG (2003) Effect of channel dimensions and shape in the flow-field distributor on the performance of polymer electrolyte membrane fuel cells. *J Power Sources* 113:11–18
15. Liu HC, Yan WM, Soong CY et al (2006) Reactant gas transport and cell performance of proton exchange membrane fuel cells with tapered flow field design. *J Power Sources* 158:78–87
16. Sun L, Oosthuizen PH, McAuley KB (2006) A numerical study of channel-to-channel flow cross-over through the gas diffusion layer in a PEM-fuel-cell flow system using a serpentine channel with a trapezoidal cross-sectional shape. *Int J Therm Sci* 45:1021–1026
17. Shimpalee S, Greenway JW, Zee Van (2006) The impact of channel path length on PEMFC flow-field design. *J Power Sources* 160:398–406
18. Wang XD, Duan YY, Yan WM et al (2008) Effects of flow channel geometry on cell performance for PEM fuel cells with parallel and interdigitated flow fields. *Electrochim Acta* 53:5334–5343
19. Hwang SY, Joh HJ, Scibioh MA et al (2008) Impact of cathode channel depth on performance of direct methanol fuel cells. *J Power Sources* 183:226–231
20. Yan WM, Li HY, Chiu PC et al (2008) Effects of serpentine flow field with outlet channel contraction on cell performance of proton exchange membrane fuel cells. *J Power Sources* 178:174–180

21. Arvay A, French J, Wang JC et al (2013) Nature inspired flow field designs for proton exchange membrane fuel cell. *Int J Hydrog Energy* 38:3717–3726
22. Currie JM (2010) Biomimetic design applied to the redesign of a PEM fuel cell flow field. MS Thesis, University of Toronto
23. Kjelstrup S, Coppens MO, Pharoah JG et al (2010) Nature-inspired energy- and material-efficient design of a polymer electrolyte membrane fuel cell. *Energy Fuels* 24:5097–5108
24. Kloess JP, Wang X, Liu J et al (2009) Investigation of bio-inspired flow channel designs for bipolar plates in proton exchange membrane fuel cells. *J Power Sources* 188:132–140
25. Wang CT, Chang CP, Shaw CK et al (2010) Fuel cell biomimetic flow slab design. *J Fuel Cell Sci Technol* 7:011009
26. Wang CT, Hu YC, Zheng PL (2010) Novel biometric flow slab design for improvement of PEMFC performance. *Appl Energy* 87:1366–1375
27. Wang M, Zheng X, Zhang Z (1998) The morphology and structure of vein. *Bull Biol* 33(8):10–12 (in Chinese)
28. Murray CD (1926) The physiological principle of minimum work. I. The vascular system and the cost of blood volume. *Proc Natl Acad Sci USA* 12:207–214
29. Murray CD (1927) A relationship between circumference and weight in trees and its bearing on branching angles. *J Gen Physiol* 10:725–729
30. Bladimir RA, Abel HG, Daniel JR (2012) Numerical investigation of the performance of symmetric flow distributors as flow channels for PEM fuel cell. *Int J Hydrog Energy* 37:436–448
31. Xu P (2008) Transport properties of fractal tree-like branching network. Ph.D. Thesis, Huazhong University of Science and Technology (in Chinese)
32. Ferziger JH, Peric M (1999) *Computational methods for fluid dynamics*, 2nd edn. Springer, Berlin
33. *Fluent 6. 3 User's Guide* (2006), Fluent Inc